Supplementary Material for Potocki et al.

Mt. Everest's highest glacier is a sentinel for accelerating ice loss

Supplementary Figure 1. South Col - Moraines shaded in red mark SCG's former extent. View from the South Col Glacier to the South. Photo by M. Potocki.

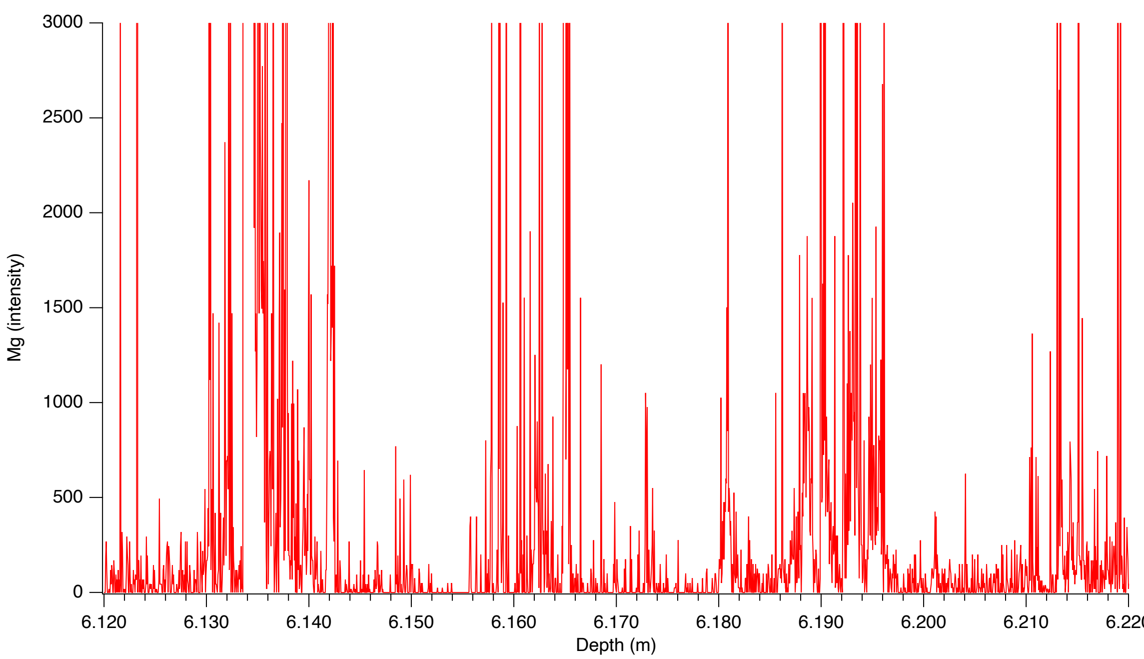

Supplementary Figure 2. **Laser data** - Example of ultra-high resolution (153 micron) laser sampling from 6.12-6.22 m depth in the SCG ice core. Winter/spring maxima in magnesium (intensity counts per second) allow the identification of net annual layering of ~27 mm w.e. a^{-1}

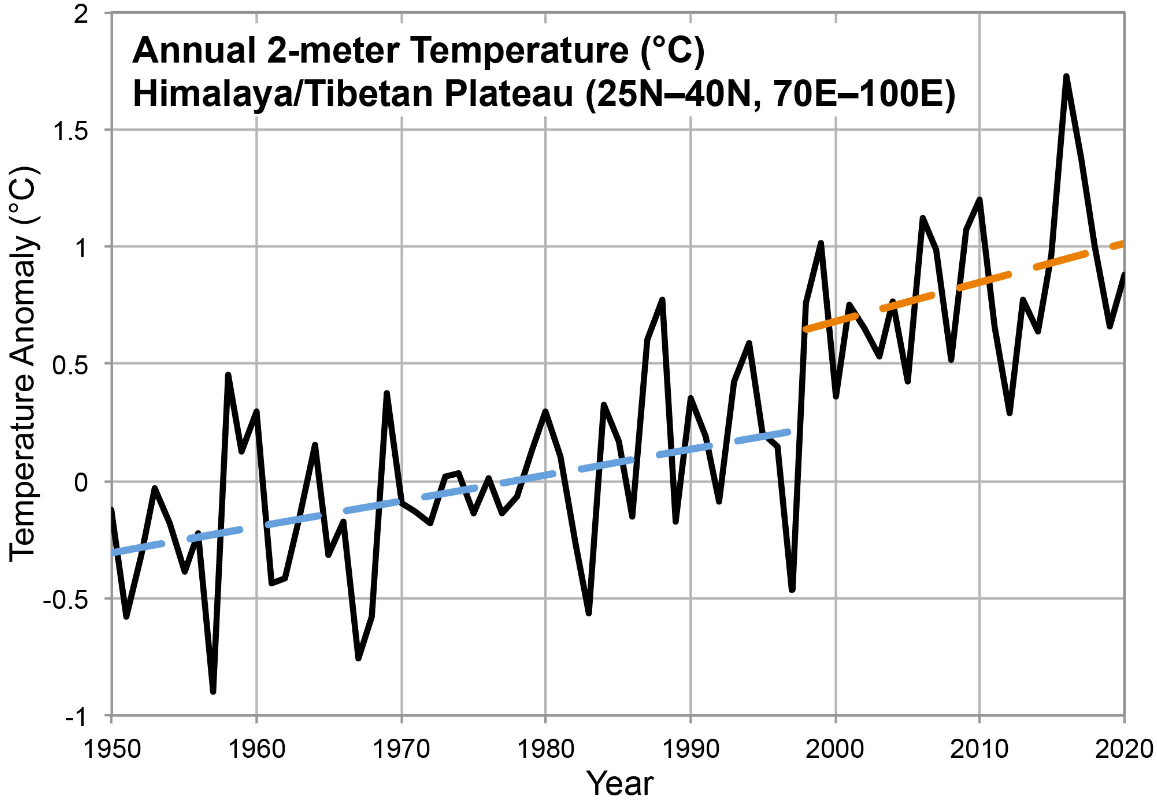

Supplementary Figure 3. Himalaya/Tibetan Plateau Temperature - Annual 2-meter temperature anomalies for the Himalaya/Tibetan Plateau region from ERA5 data[1] for the period 1950–2020. The anomalies are relative to a 1950–2000 climatology. Linear trendlines are overlain for the early (1950–1997) and late (1998–2020) portions of the record to highlight an abrupt change in baseline temperature after the 1997/98 El Niño.

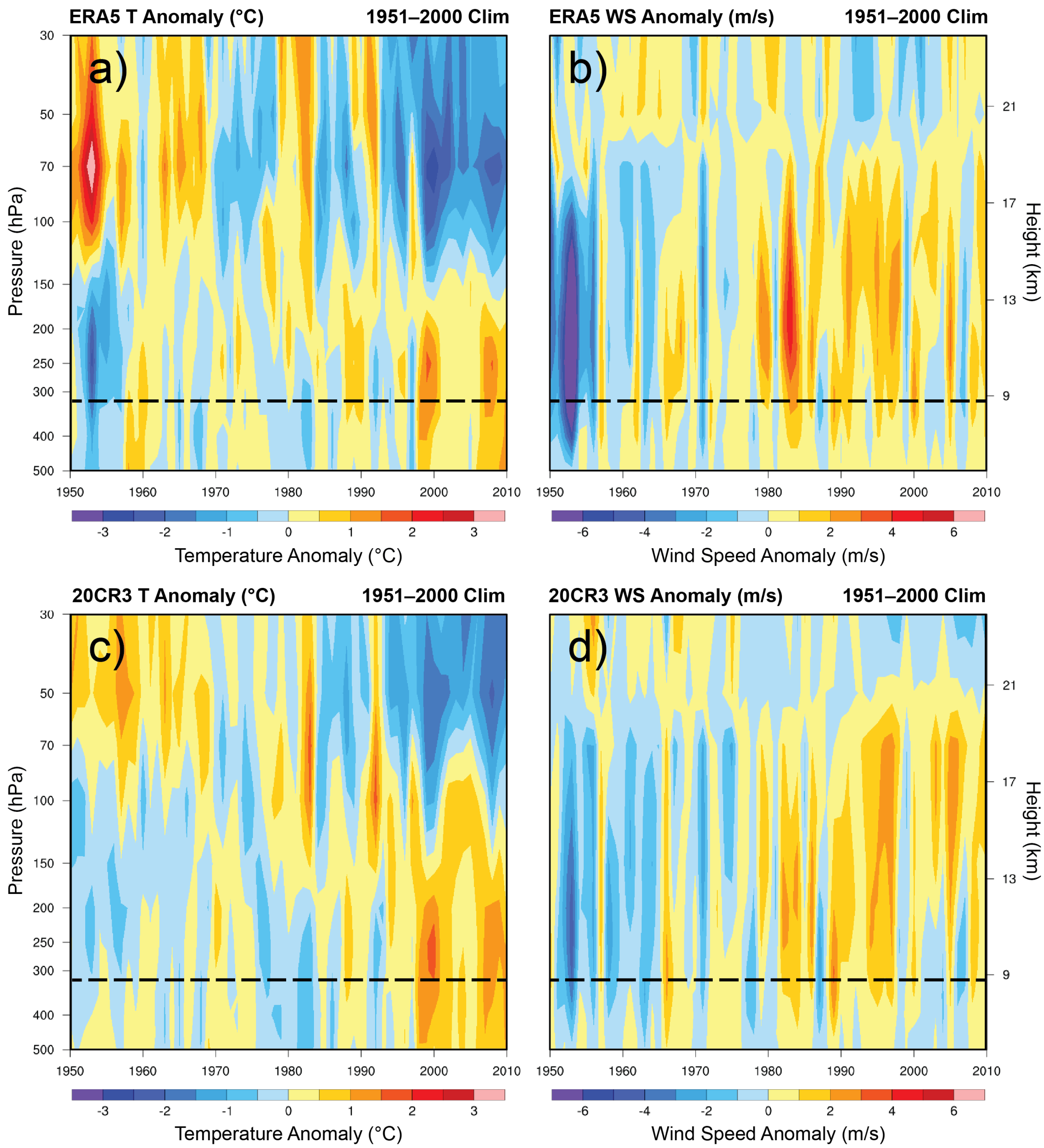

Supplementary Figure 4. Vertical **Temperature and Wind over Everest** - Comparison of temperature (a, c) and wind speed (b, d) time/height profiles over Mt. Everest from ECMWF ERA-5[1] (top) and NOAA Twentieth Century Reanalysis Version 3[2] (bottom). The dashed line indicates the approximate level of Mt. Everest summit. Annual anomalies are relative to 1951–2000 climatology. Generated using Climate Reanalyzer[3] (CCI, 2021).

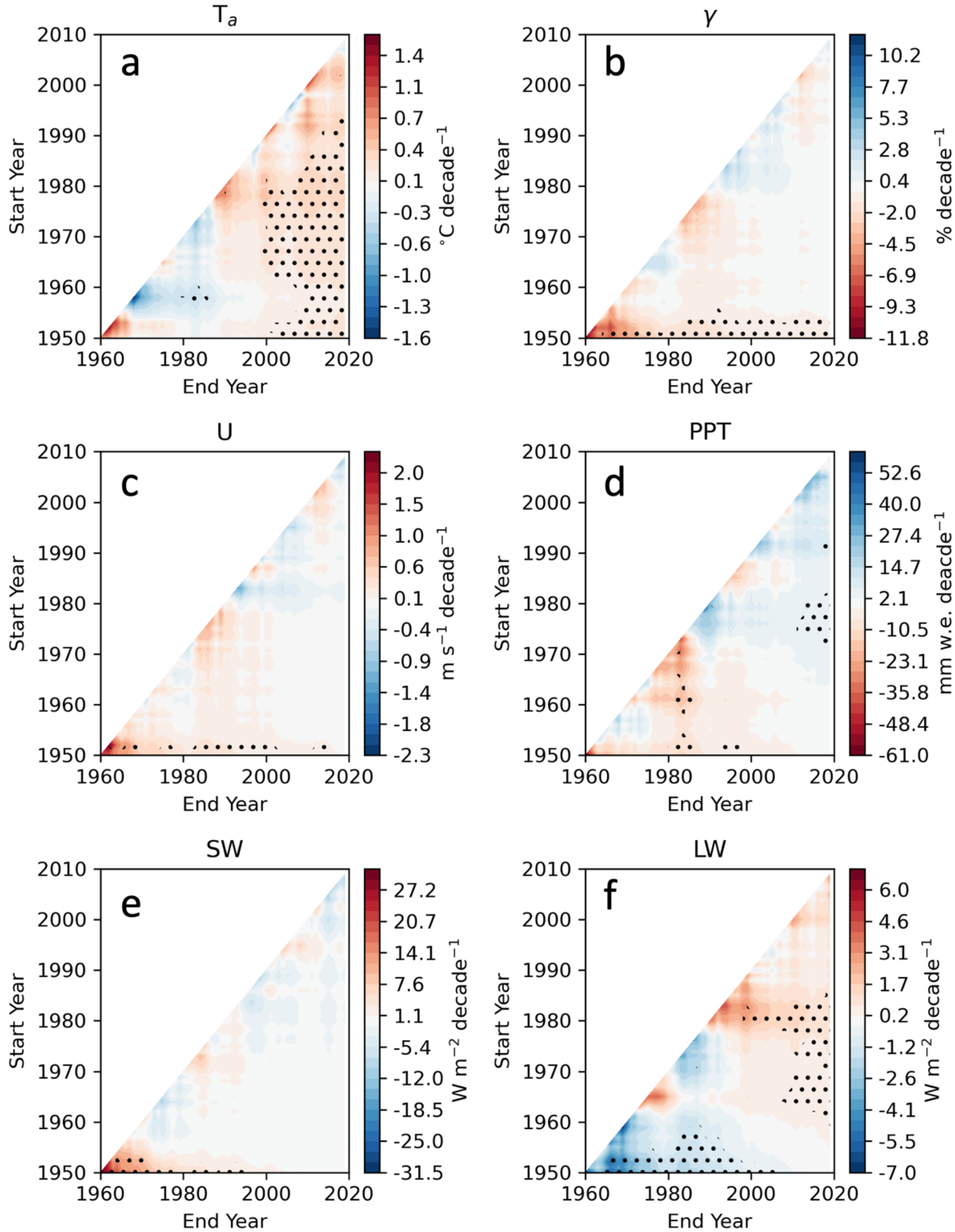

Supplementary Figure 5. Trends in Meteorological Variables - Non-parametric Theil-Sen[4,5] trends in annual means of the meteorological variables for different combinations of start and end years: (a) air temperature, (b) relative humidity, (c) wind speed, (d) precipitation, (e) incident shortwave radiation, and (f) incident longwave radiation. Hatched regions show trends that are significantly different from zero (p<0.05).

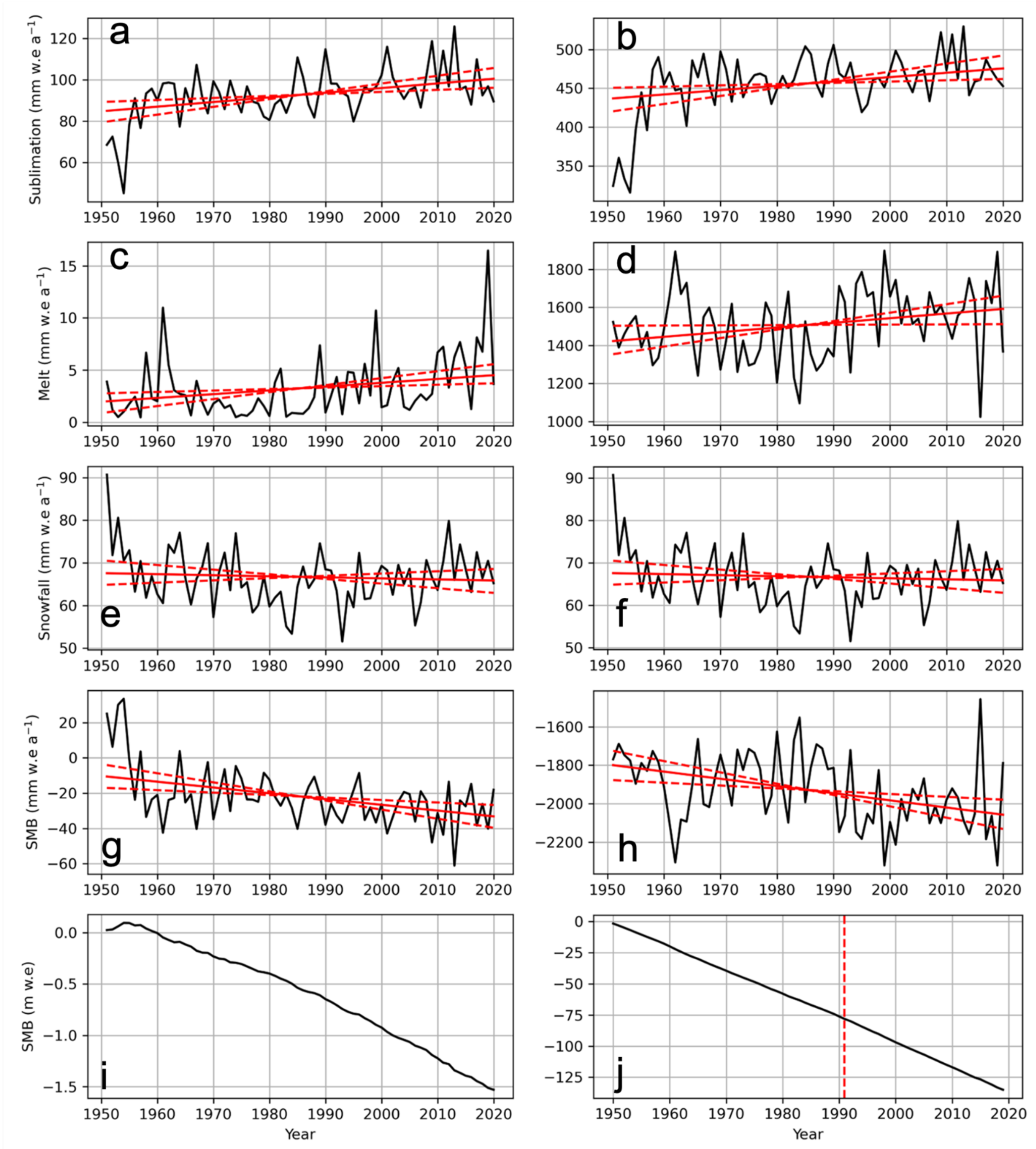

Supplementary Figure 6. Model Simulations - COSIPY simulated mass balance for a snow surface (left column) and an ice surface (right column): (a-b) sublimation, (c-d) melt, (e-f) snowfall, (g-h) surface mass balance, and (i-j) cumulative surface mass balance. The solid red lines (in panels a-h) show median Theil-Sen slope estimates, and the dashed lines show the 95% confidence interval. The vertical dotted red lines in panel j highlights the year (1994) from which an additional ~55 m w.e. is lost by the beginning of 2019.

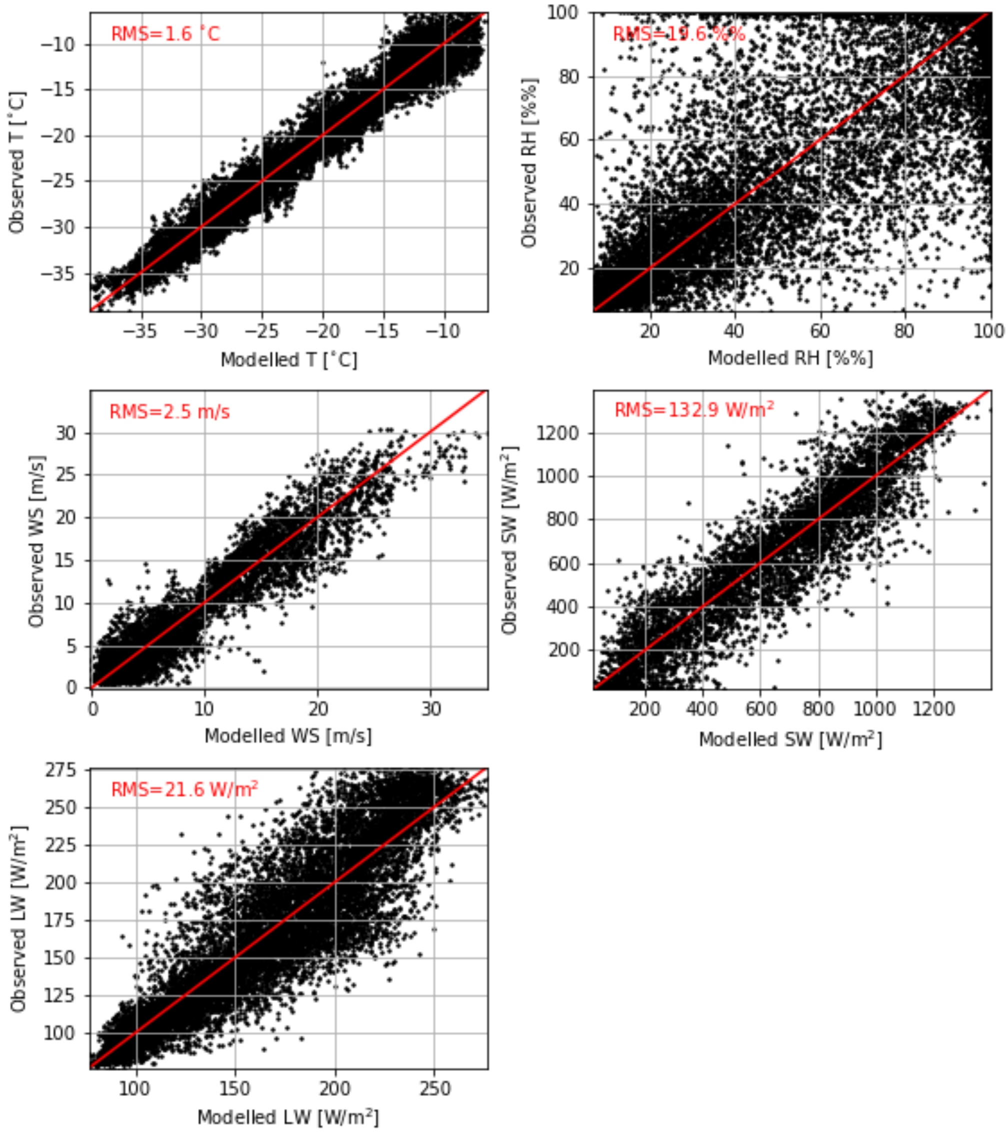

Supplementary Figure 7. Hourly ERA5 Downscaled Meteorology vs. Observations- Comparison of the observed and reconstructed variables modelled through the five-fold cross-validation procedure.

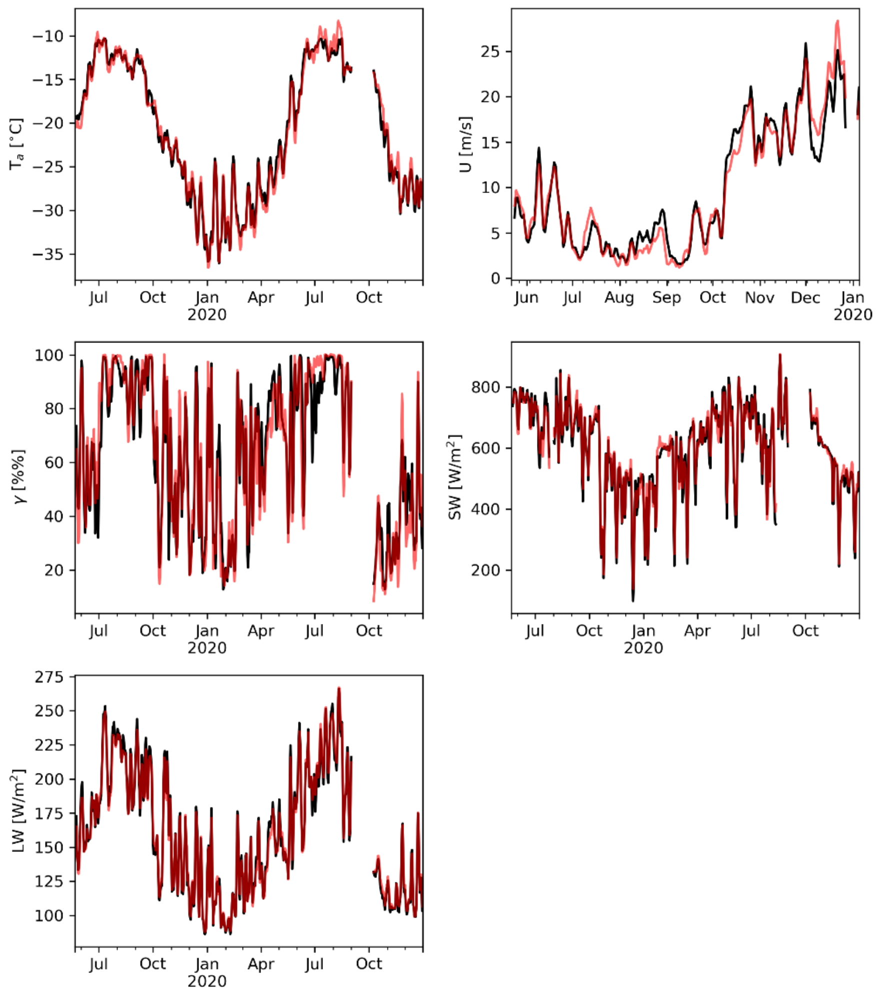

Supplementary Figure 8. ERA5 Downscaled and Observed Meteorology - Comparison of the observed (black) and reconstructed (red) variables modelled through the five-fold cross-validation procedure and smoothed with a three-day moving window.

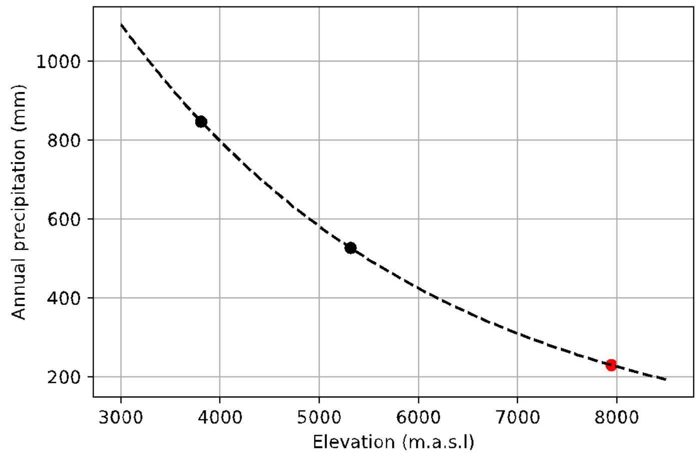

Supplementary Figure 9. Precipitation vs Elevation - Relationship between liquid equivalent annual precipitation and elevation. Black dots are the 2020 annual precipitation at the Phortse (3810 m) and Basecamp (5315 m) AWSs. Dotted line is the calibrated exponential regression, and the red dot is the result of using this regression to estimate annual precipitation at the South Col AWS (7,945 m).

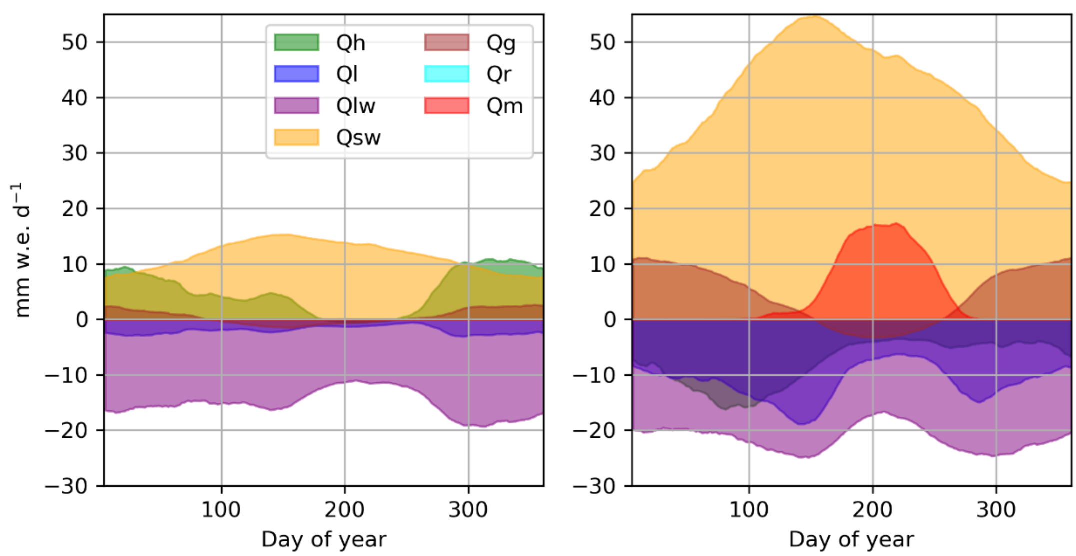

Supplementary Figure 10. Snow and Ice Comparison - Day-of-year mean energy fluxes converted to mm w.e. d^{-1} (multiplied by the number of seconds in one day and divided by the latent heat of fusion) for the snow (left) and ice (right) COSIPY simulations. See Equation 1 in the main text (Methods) for the notation used to identify the respective energy fluxes.

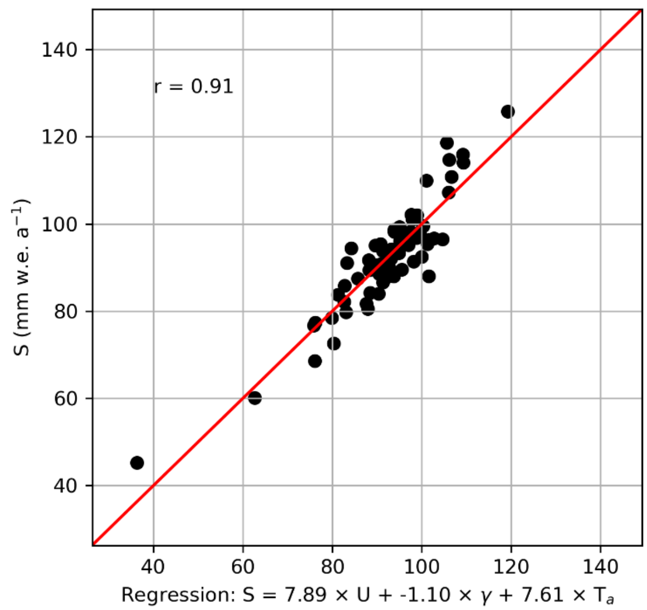

Supplementary Figure 11. **Sublimation** - Annual snow sublimation modelled via multiple linear regression (x-axis) versus annual sublimation from the COSIPY snow simulation (y-axis). Note that values for the regression coefficients are shown on the x-axis label.

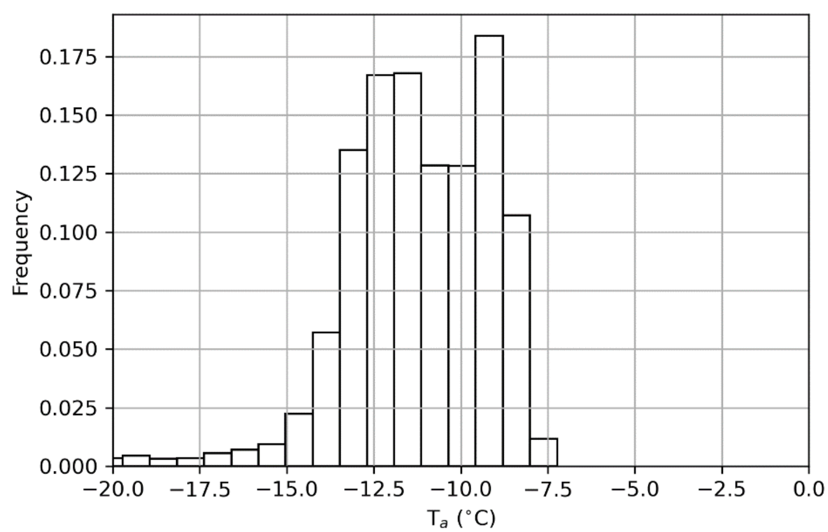

Supplementary Figure 12. **Surface Melt Events** - Normalized frequency of hourly-mean 2 m air temperatures during surface melt events in the COSIPY snow simulation. Bin counts are weighted by melt energy.

Uncertainty Assessment in COSIPY simulations

We generated an ensemble of model runs differentiated by perturbations to key COSIPY parameters, following the “crystallizing “approach to uncertainty characterization[6]. The bounds of parameter values were changed in turn, with their limits informed by another application of mass balance modelling in High Mountain Asia[7]. For each of these perturbation runs, we repeated the strategy described in the main paper (Methods), scaling the precipitation so that the SCG was in mass balance for the 1950-1959 snow simulation We then summarized the effect of the respective perturbation by taking the cumulative surface mass balance (CMB) at the end of the simulation period (1950-2019). This univariate assessment was then used to inform an estimate of the combined effects of parameter uncertainty. We used the results from changing the parameters in isolation to inform the combination expected to generate the maximum and minimum CMB. The results of this assessment (Table S1) indicate that whilst parameter uncertainty impacts the magnitude of the snowpack thinning and rate of loss when glacier ice is exposed, it does not qualitatively affect our conclusions.

Supplementary Table 1. Uncertainty characterization in the snow and ice COSIPY simulations. “High and “Low” ice and snow cumulative mass balance (CMB) correspond to the values reached at the end of the simulation period (1950-2019) when COSIPY was run with the respective “High” or “Low” parameter values. [1]z_0 denotes the roughness length for momentum. [2]Indiates use of Monin-Obukhov similarity theory to compute a stability correction in the turbulent heat fluxes (instead of the default correction applied based on the bulk Richardson number). [3,4]See Supplementary Table 2 for parameter settings used for model runs attempting to minimize and maximize CMB over the simulation period.

Parameter [units]	**High**	**Low**	**High snow CMB (m w.e)**	**Low snow CMB (m w.e.)**	**High ice CMB (m w.e.)**	**Low ice CMB (m w.e.)**
Albedo fresh snow [-]	0.88	0.82	-1.25	-1.92	-135	-140
Albedo firn [-]	0.6	0.5	-1.48	-1.52	-135	-135
Albedo ice [mm]	0.5	0.3	-	-	-84	-191
[1]z_0 snow **[mm]**	0.29	0.19	-1.61	-1.41	-135	-135
z_0 firn **[mm]**	6.5	1.5	-1.53	-1.53	-134	-134
z_0 ice [mm]	2.7	0.7	NA	NA	-129	-147
[2]MO stability	on		-1.43		-116	
[3]Combined snow	-		-2.05	-1.14	-	
[4]Combined ice	-		-	-213	-67	

Supplementary Table 2. Parameter settings for combination runs expected to generate the maximum and minimum CMB over the COSIPY snow and ice simulations.

Snow		
Parameter [units]	**Perturbed high (max ablation)**	**Perturbed low (min ablation)**
Albedo fresh snow [-]	0.82	0.88
Albedo firn [-]	0.5	0.6
z_0 snow [mm]	0.29	0.19
z_0 firn [mm]	6.5	1.5
MO stability	off	on
Ice		
Albedo fresh snow [-]	0.82	0.88
Albedo firn [-]	0.5	0.6
Albedo ice [-]	0.3	0.5
z_0 snow [mm]	0.19	0.29
z_0 firn [mm]	1.5	6.5
z_0 ice [mm]	0.7	2.7
MO stability	off	on

Supplementary References:

1. Hersbach, H., Bell, B., Berrisford, P., Hirahara, S., Horányi, A., Muñoz-Sabater, J., Nicolas, J., Peubey, C., Radu, R., Schepers, D. and Simmons, A. (2020), The ERA5 global reanalysis. *Quart. J. Roy. Meteor. Soc.*, **146**, 1–51, https://doi.org/10.1002/qj.3803
2. Slivinski, L.C., Compo, G.P., Whitaker, J.S., and 43 co-authors (2019), Towards a more reliable historical reanalysis: Improvements for version 3 of the Twentieth Century Reanalysis system. Quart. J. Roy. Meteor. Soc., 145 (724), 2876–2908, https://doi.org/10.1002/qj.3598
3. CCI, 2021. Climate Reanalyzer is a climate data access and visualization tool developed by the Climate Change Institute at the University of Maine. Maps of monthly reanalysis data from several models can be generated using the interface at https://climatereanalyzer.org/reanalysis/monthly_maps/.
4. Theil, H., 1950, A rank-invariant method of linear and polynomial regression analysis. I, II, III I, II, III", Proceedings van de Koninklijke Nederlandse Akademie van Wetenschappen 53: 386–392, 521–525, 1397–1412.
5. Sen, P.K., 1968, Estimates of the Regression Coefficient Based on Kendall's Tau. Journal of the American Statistical Association, 63, 1379-1389, http://dx.doi.org/10.1080/01621459.1968.10480934
6. Smith, K.A., Wilby, R.L., Broderick, C., Prudhomme, C., Matthews, T., Harrigan, S. and Murphy, C., 2018. Navigating cascades of uncertainty—as easy as ABC? Not quite….*Journal of Extreme Events*, *5*(01), p.1850007, https://doi.org/10.1142/S2345737618500070

7. Mölg, T., Maussion, F., Yang, W. and Scherer, D., 2012. The footprint of Asian monsoon dynamics in the mass and energy balance of a Tibetan glacier. *The Cryosphere*, *6*(6), pp.1445-1461, https://doi.org/10.5194/tc-6-1445-2012